Part III

Sub-harmonic Faraday waves in circular cylinders and thin annuli

Introduction

Orderly and intricate structures often emerge from basic building blocks in nature, such as the crystallization of water molecules into snowflakes or the self-assembly of nucleotides into complex DNA structures. Sand also piles into patterns of ripples or stripes in the desert, showcasing a more diligent and efficient creation process than many human approaches that require piece-by-piece construction.

The assembling of microscale materials has been receiving increasing attention due to high demands in engineering architectures and systems across various fields such as tissue engineering (Athanasiou et al., 2013; Gurkan et al., 2012), microelectromechanical systems (Knuesel and Jacobs, 2010; Stauth and Parviz, 2006), and micro-photonics (Lu et al., 2001). For instance, tissue engineering is particularly interesting as it involves organizing cells into repeating units with well-defined 3D architectures to achieve tissue-specific functions necessary for various applications.

In the context of microscale technologies, several methods are nowadays available for creating various structures using microscale materials. Among those, Chen et al. (2014) presented a highly adaptable and biocompatible method for generating a wide range of structures using microscale materials (see figure III.1). By leveraging the topography of liquid surfaces created by standing waves, they could direct the assembly of a large number of microscale materials into various ordered and symmetric structures. This liquid-based template can be dynamically reconfigured in a very short time (in the order of a few seconds) and allows for scalable and parallel assembly. Moreover, they demonstrated that the assembled structures can be immobilized through chemical- and photo-crosslinking for subsequent use.

In this technique, standing wave patterns are generated by imposing to a partially filled container a vertical harmonic forcing, with an amplitude above a critical threshold, so as to trigger parametric Faraday waves (see also Chapter 1). It is therefore crucial to characterize and predict the hydrodynamics at stake and, particularly, the instability onset of these waves.

In the following, we give an overview of the origin of the Faraday instability. Specifically, we discuss the classical theoretical frameworks typically employed in the prediction and characterization of such standing wave patterns, with a particular focus on some important limitations and oversimplifications of these models. The latter will indeed motivate the studies carried out in Chapters 7 and 8.

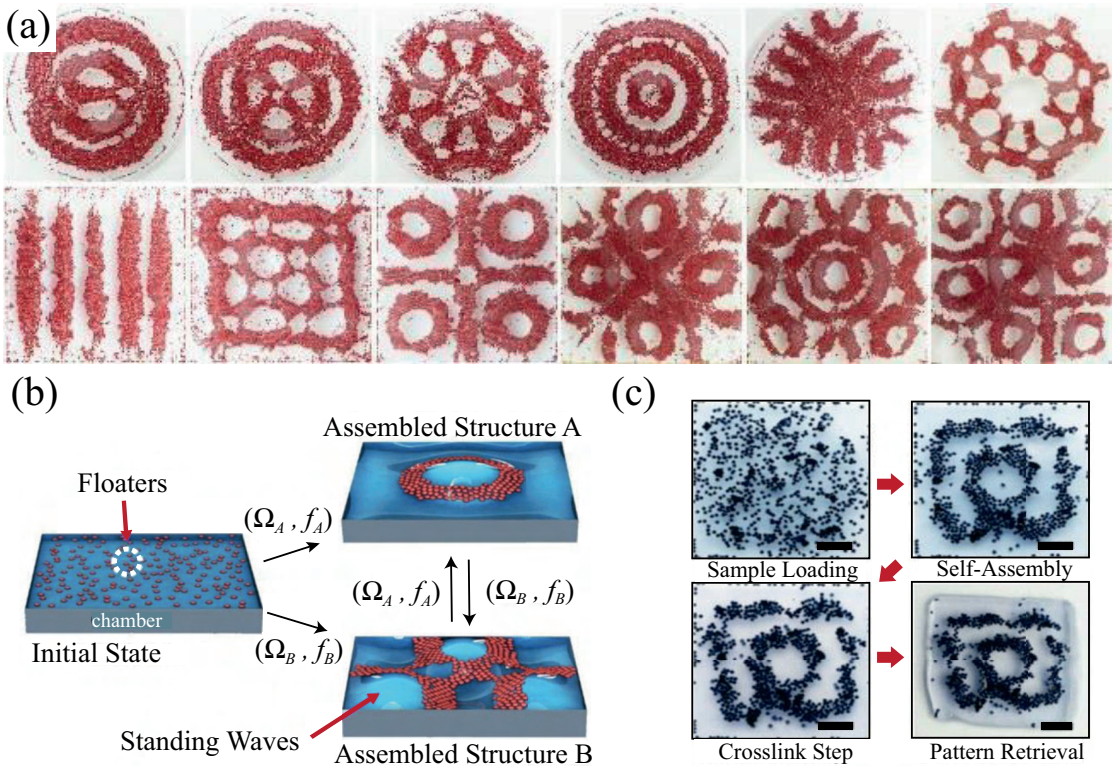

Figure III.1 – Dynamical reconfigurability of liquid-based templated assembly (figure modified from (Chen et al., 2014)). (a) Chamber shape effect on the assembly: circular (*top*) versus squared (*bottom*) vessels. (b) A schematic of dynamic reconfiguration of the assembled structures: (fA, aA) and (fB, aB) are vibrational frequencies and accelerations for the formation of structures A and B, respectively. (c) Photo crosslinking of the assembled structure. Once the hydrogels were assembled, crosslinking was performed to immobilize the assembled pattern. Scale bars: 4 mm.

When a vessel containing liquid undergoes periodic vertical oscillations, the free liquid surface may be parametrically destabilized with the excitation of standing waves depending on the combination of forcing amplitude and frequency. The threshold at which the instability appears is a function of the corresponding mode dissipation and the excited wavelength is generally specified by the wave whose natural frequency is half that of the parametric excitation, as first noticed by Faraday (1831), who observed experimentally that the resonance was typically of sub-harmonic nature. This observation was later confirmed by Rayleigh (1883a,b), in contrast with Matthiessen (1868, 1870), who observed synchronous vibrations of the free surface with the vertical shaking. The pioneering work of Benjamin and Ursell (1954) gave momentum to the theoretical investigations of the Faraday instability. Using first principles, Benjamin and Ursell (1954) determined the linear stability of the flat free surface of an ideal fluid within a vertically vibrating container displaying a sliding contact line which intersects orthogonally the container sidewalls. The stability is governed by a system of uncoupled Mathieu equations (see Chapter 1), which predict that standing capillary-gravity waves appear

inside the so-called Faraday tongues in the driving frequency-amplitude space, with the wave response that can be sub-harmonic, harmonic or super-harmonic, hence reconciling previous observations.

Dissipation in absence of walls

The effect of viscous dissipation, taken to be linear and sufficiently small, was initially introduced heuristically (Lamb, 1993; Landau and Lifshitz, 1959) in the inviscid solution, resulting in a semi-phenomenological damped Mathieu equation, which was later proven by the viscous linear Floquet theory of Kumar and Tuckerman (1994b) to be inaccurate, even at small viscosities. An improved version of the damped Mathieu equation, accounting in a more rigorous manner for the dissipation taking place in the free surface and bottom boundary layer, was proposed by Müller et al. (1997), who also noticed in their experiments that the fluid depth can affect the Faraday threshold, with harmonic responses most likely to be triggered for thin fluid layers. The viscous theory of Kumar and Tuckerman (1994b), formulated for a horizontally infinite domain, was found to give good agreement with the small-depth large-aspect-ratio experiments of Edwards and Fauve (1994), where the influence of lateral walls was negligible. If indeed, at large excitation frequencies, where the excited wavelength is much smaller than the container characteristic length, the accessible range of spatial wavenumber is nearly continuous, in the low-frequency regime of single-mode excitation the mode quantization owing to the container sidewall becomes a dominant factor, leading to a discrete spectrum of resonances.

Mobile contact lines

A generalization of the viscous Floquet theory to spatially finite systems can be readily obtained by analogy with the inviscid formulation of Benjamin and Ursell (1954), as Batson et al. (2013) recently proposed (see figure III.2(a)). It has however intrinsic limitations as it relies on ideal lateral wall conditions, i.e. the unperturbed free surface is assumed to be flat, the contact line is ideally free to slip with a constant zero slope and the stress-free sidewall boundary condition is required for mathematical tractability, since it allows for convenient Bessel-eigenfunctions representation. With the noticeable exception of the sophisticated experiments by Batson et al. (2013) and Ward et al. (2019) using a gliding liquid coating, these assumptions, by overlooking the contact line dynamics, lead in most experimental cases to a considerable underestimation of the actual overall dissipation, resulting in many cases in an inaccurate prediction of the linear Faraday thresholds in small-container experiments (Benjamin and Ursell, 1954; Ciliberto and Gollub, 1985; Das and Hopfinger, 2008; Dodge et al., 1965; Henderson and Miles, 1990; Tipton and Mullin, 2004). The complexity lies primarily in the region of the moving contact line, where molecular, boundary layer and macroscopic scales are intrinsically connected. Despite the significant efforts devoted by several authors to its theoretical understanding (Case and Parkinson, 1957; Cocciaro et al., 1993, 1991; Davis, 1974; Hocking, 1987; Jiang et al., 2004; Keulegan, 1959; Miles, 1967, 1990, 1991; Perlin and Schultz, 2000; Ting and Perlin, 1995), the

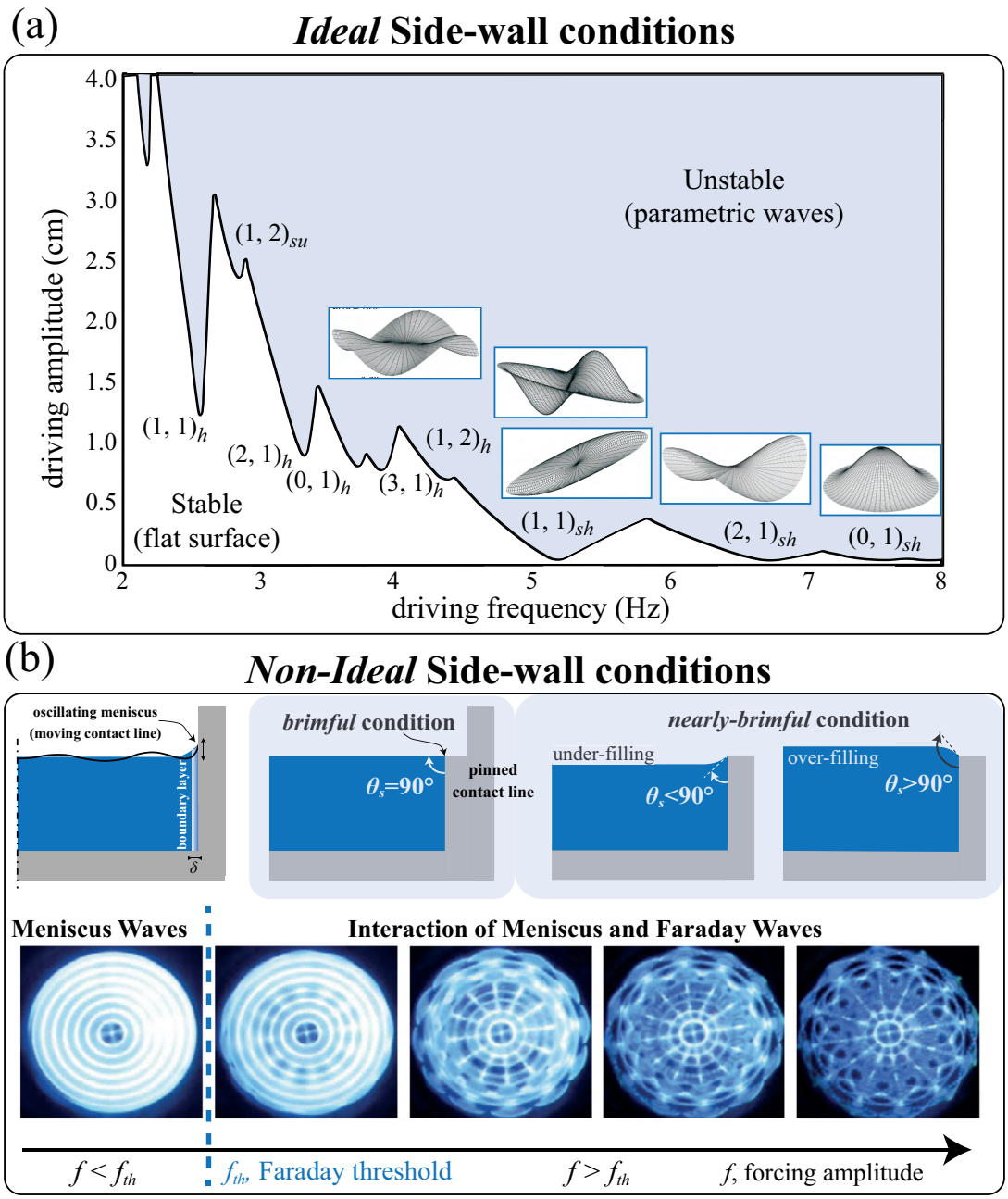

Figure III.2 – (a) Stability map in the driving parameter space computed via Floquet analysis by Batson et al. (2013) for a bi-layer fluid system in a small cylindrical container and assuming *ideal* sidewall conditions: flat static surface and stress-free sidewall, i.e. the viscous boundary layer at the lateral wall is neglected and the static contact angle is ideally assumed $\theta_s = 90°$. The insets show few free surface shapes. (b) A way to eliminate the static meniscus is to fill the container up to the rim (*brimful*). This configuration also allows one to control the shape and size of the meniscus by slightly underfilling or overfilling the container (*nearly-brimful* condition, $\theta_s \neq 90°$). An oscillating meniscus emits meniscus waves, which have a zero threshold, oscillate harmonically with the forcing and appears as concentric ripples. For forcing amplitudes f above the Faraday threshold, f_{th}, those waves interact with the parametric waves and produce new patterns.

comparison with moving-contact-line experiments, due to unavoidable sources of uncertainty in the meniscus dynamics, remained mostly qualitative, rather than quantitative, requiring often the use of fitting parameters, e.g. a larger effective fluid viscosity (Henderson and Miles, 1990).

Pinned contact lines

A natural means to get rid of the extra dissipation produced by the contact line dynamics is to simply pin the free surface at the edge of the sidewall, i.e. the container is filled to the brim (brimful condition), as shown in figure III.2(b)). In such a condition, the overall dissipation is ruled by that occurring in the fluid bulk and in the Stokes boundary layers at the bottom and at the solid lateral walls, where the fluid obeys the classic no-slip boundary condition, relaxing the stress-singularity at the contact line (Davis, 1974; Huh and Scriven, 1971; Lauga et al., 2007; Miles, 1990; Navier, 1823; Ting and Perlin, 1995). Even in the inviscid context, the problem of a pinned contact line boundary condition is well-posed, as shown by the seminal works of Benjamin and Scott (1979) and Graham-Eagle (1983), who first solved the resulting dispersion relation for inviscid capillary-gravity waves with a free surface pinned at the container brim using a variational approach and a suitable Lagrange multiplier. Since then, several semi-analytical techniques, often combining an inviscid solution with boundary layer approximations and asymptotic expansions accounting for viscous dissipation, have been therefore developed to solve the pinned contact line problem, for example in cylindrical containers (Henderson and Miles, 1994; Kidambi, 2009b; Martel et al., 1998; Miles and Henderson, 1998; Nicolás, 2002, 2005). The resulting predictions of natural frequencies and damping coefficients of these capillary-gravity waves, in contradistinction with the case of a moving contact line, showed a remarkable agreement with experimental measurements (Henderson and Miles, 1994; Howell et al., 2000).

Ubiquity of Meniscus waves

Within the framework of the Faraday instabilities, this pinned contact line condition can be reached by carefully filling up the vessel to the brimful condition, as done by Douady (1990) and Edwards and Fauve (1994), among others. Nevertheless, as noticed by Bechhoefer et al. (1995), these delicate experimental conditions are not always perfectly achieved, leading to the presence of a minute meniscus. As mentioned for instance by Douady (1990), the meniscus cannot remain steady upon the oscillating vertical motion of the vessel, which results in the emission of travelling waves from the sidewall to the interior. Irrespective of the pinned or free-edge nature of the contact line, these so-called *meniscus waves* are synchronized with the excitation frequency. They are not generated by the parametric resonance, but rather by the modulation of the gravitational acceleration resulting in an oscillating capillary length. They do not need to overcome a minimal threshold in forcing amplitude to appear, are therefore observable in the whole driving frequency-amplitude space and are well described by a purely linear response, i.e. at sufficiently small forcing amplitude, the meniscus-wave amplitude is

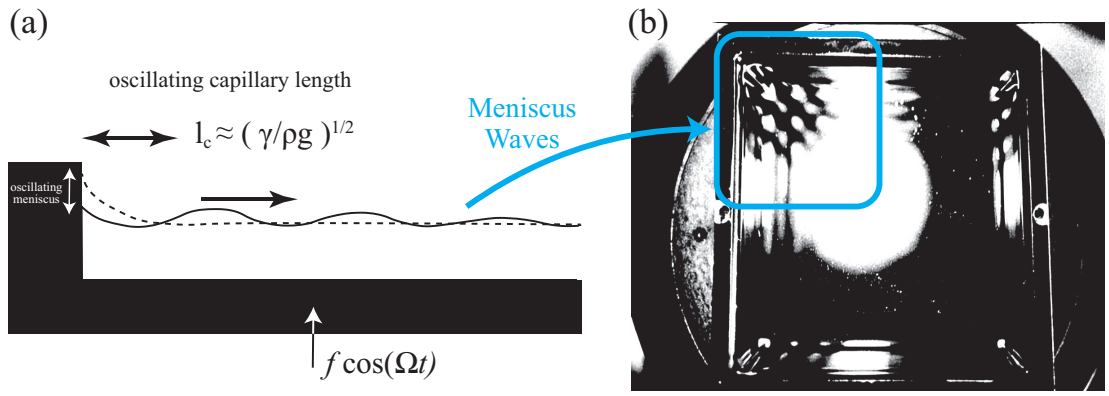

Figure III.3 – (a) A meniscus, the typical length of which is the capillary length $l_c = (\gamma/\rho g)^{1/2}$, with γ the liquid surface tension, ρ the liquid density and g the gravity acceleration, is always excited by a vertical oscillation. When the cell goes up, the effective gravity is increased and the meniscus length decreases. So it emits a surface wave in order to preserve the mass. For a vertical oscillation of the vessel, the meniscus thus produces an isochronous wave. (b) Photograph of a wave emitted by the meniscus of an oil layer of depth $h = 2\,\text{mm}$, in a square cell $80 \times 80 \times 5\,\text{mm}^2$, at a forcing frequency of 20 Hz, visualized by the vertical reflection of a light beam. The waves are clearly generated from the boundaries and quickly damped so that the center of the cell is still flat. Without any meniscus, the surface remains flat even during vertical oscillation (Douady, 1990).

proportional to the external forcing amplitude.

As stated by Douady (1990), edge waves constitute a new time-dependent base state on which the instability of parametric waves may develop, possibly blurring the experimental detection of the true Faraday thresholds (see figure III.3). This has led researchers to attempt to suppress edge waves by selecting large-aspect-ratio containers where sidewall effects are negligible, using *sloping sides* or *shelf* conditions to mitigate edge waves by impedance matching (Bechhoefer et al., 1995), or employing highly viscous fluid which damps out these waves (Bechhoefer et al., 1995; Douady, 1990).

With interests in pattern formation, pure meniscus-waves-patterns were investigated for themselves by Torres et al. (1995), while complex patterns originated by the coupling of meniscus and Faraday waves were recently described by Shao et al. (2021a,b) for small circular-cylinder experiments. A discussion about harmonic Faraday waves disturbed by harmonic meniscus waves is also outlined in Batson et al. (2013), where the presence of edge waves in a small circular-cylinder-bilayer experiment leads to an imperfect bifurcation diagram, also referred to as a tailing effect by Virnig et al. (1988), who analyzed sub-harmonic responses only. Interestingly, in some cases, e.g. liquid-based biosensors for DNA detection (Picard and Davoust, 2007), tunable small-amplitude stationary waves as meniscus waves are actually desired and preferred to saturated larger-amplitude Faraday waves. In such applications, a starting brimful condition, having a contact line fixed at the brim, is ideal since the effective static contact angle at the wall and hence the size and shape of the static meniscus, which will emit edge waves under vertical excitations, can be adjusted simply by increasing or decreasing

the bulk volume (*nearly–brimful* condition, see figure III.2(b)).

Although the non-conventional eigenvalue problem for natural frequencies and damping coefficients of pinned-contact-line capillary-gravity waves was tackled by several authors mentioned above and in spite of the vastness of literature focused on Faraday waves, there is a lack of a comprehensive theoretical framework for the investigation of such a configuration within the context of Faraday instability.

An important exception is the work of Kidambi (2013). Assuming inviscid Faraday waves in a brimful cylinder with an ideally flat static free surface, he represented the problem using appropriate modal solutions followed by a projection on a test function space and showed that pinned contact line condition resulted in an infinite system of coupled Mathieu equations, unlike the classic case of an ideal moving contact line (Benjamin and Ursell, 1954). Nevertheless, viscosity, crucial for an accurate prediction of the Faraday threshold and the associated emergence of the standing wave pattern, was not included in the analysis, nor was the presence of a static meniscus and its consequent emission of meniscus waves. Some attempts to include meniscus modifications to the Faraday thresholds have been made by several authors by including periodic inhomogeneities (Ito et al., 1999; Tipton, 2003) and phenomenological terms (Lam and Caps, 2011) to an *ad hoc* damped Mathieu equation.

Following this literature survey, the purpose of **Chapter 7** is to take one more step in the direction undertaken by Kidambi (2013), by rigorously accounting for (i) viscous damping, (ii) a pinned contact line and (iii) the presence of a static meniscus at rest. As mentioned above, a contact angle different from 90 degrees not only results in a static meniscus but also induces the emission of meniscus waves as the static meniscus shape is no longer a solution to the forced problem, even below the Faraday threshold. A Floquet-inspired linear theory *à la* Kumar and Tuckerman (1994b) cannot be pursued, as perturbations develop around an oscillating base flow. In contrast, we propose to use the weakly nonlinear approach (WNL) to approximate the linear Faraday bifurcations, although it is expected to involve cumbersome calculations.

Weakly nonlinear analysis

Weakly nonlinear analyses (Chen and Vinals, 1999; Douady, 1990; Henderson and Miles, 1990; Jian and Xuequan, 2005; Meron and Procaccia, 1986; Miles, 1984b; Milner, 1991; Nagata, 1989; Nayfeh, 1987; Rajchenbach and Clamond, 2015a; Skeldon and Guidoboni, 2007; Zhang and Vinals, 1997) have indeed been widely used in the context of Faraday instabilities to study the wave amplitude saturation via super and subcritical bifurcations, as well as to investigate pattern and quasi-pattern formation (Edwards and Fauve, 1994; Stuart and Fauve, 1993) or spatiotemporal chaos (Ciliberto and Gollub, 1985; Gluckman et al., 1993), arising when two modes with nearly the same frequency share the same unstable region in the parameter space and strongly interact. In contradistinction to these previous studies, the presence of a static meniscus calls for a WNL approach not only to estimate the wave amplitude saturation in

the weakly nonlinear regime but also to predict the Faraday threshold. Hence, with regard to cylindrical straight-sidewalls and sharp-edged containers, as the one considered by Shao et al. (2021b), we derive a WNL model capable of simultaneously accounting for viscous dissipation, static meniscus and meniscus waves, thus allowing us to predict their influence on the linear Faraday threshold for standing capillary-gravity waves with pinned contact line as well as their saturation to finite amplitude. Following the recent experimental evidence of Shao et al. (2021b), we focus on single-mode sub-harmonic resonances. To this end, the full system of equations governing the fluid motion is solved asymptotically by means of the method of multiple timescales, involving a series of linear problems, which are solved numerically. The theoretical model results in a final amplitude equation for the wave amplitude, B, whose form corresponds to that derived by Douady (1990) using symmetry arguments solely and keeping low order terms only,

$$\frac{dB}{dt} = -(\sigma + \mathrm{i}\Lambda/2)\, B + \zeta F B^* + \nu |B|^2 B.$$

where σ is the damping coefficient, Λ is the frequency-detuning parameter and the star symbol denotes the complex conjugate. This equation correctly predicts the existence of a so-called sub-harmonic Faraday tongue in the driving frequency-amplitude (i.e. the Ω_d-F_d) plane. Within the tongue, the forced response driven at Ω_d is linearly unstable and a solution oscillating ω (which is sufficiently close to $\Omega_d/2$) emerges. The equation above is indeed valid whatever the shape of the static surface, mode structure and the boundary condition are, but the normal form coefficients ζ and ν, which account for the effect of the static contact angle and which are complex values owing to the presence of viscosity, are here formally determined in closed form from first principles and computed numerically.

Faraday waves in Hele-Shaw cells

When it comes to Faraday waves in Hele-Shaw cells, it is even more crucial to pay close attention to the treatment of the sidewall and contact line conditions, as these factors play a dominant role in this configuration.

Recent Hele-Shaw cell experiments have enriched the knowledge of Faraday waves (Faraday, 1831). Researchers have uncovered a new type of highly localized standing waves, referred to as oscillons, that are both steep and solitary-like in nature (Rajchenbach et al., 2011) (see figure III.4(a,b)). These findings have spurred further experimentations with Hele-Shaw cells filled with one or more liquid layers, using a variety of fluids, ranging from silicone oil, and water-ethanol mixtures to pure ethanol (Li et al., 2018b) (figure III.4(c)). Through these experiments, new combined structures produced by triadic interactions of oscillons were discovered by Li et al. (2014) (figure III.4(d,e)). Additionally, another new family of waves was observed in a cell filled solely with pure ethanol and at extremely shallow liquid depths (Li et al., 2016, 2015) (figure III.4(f)).

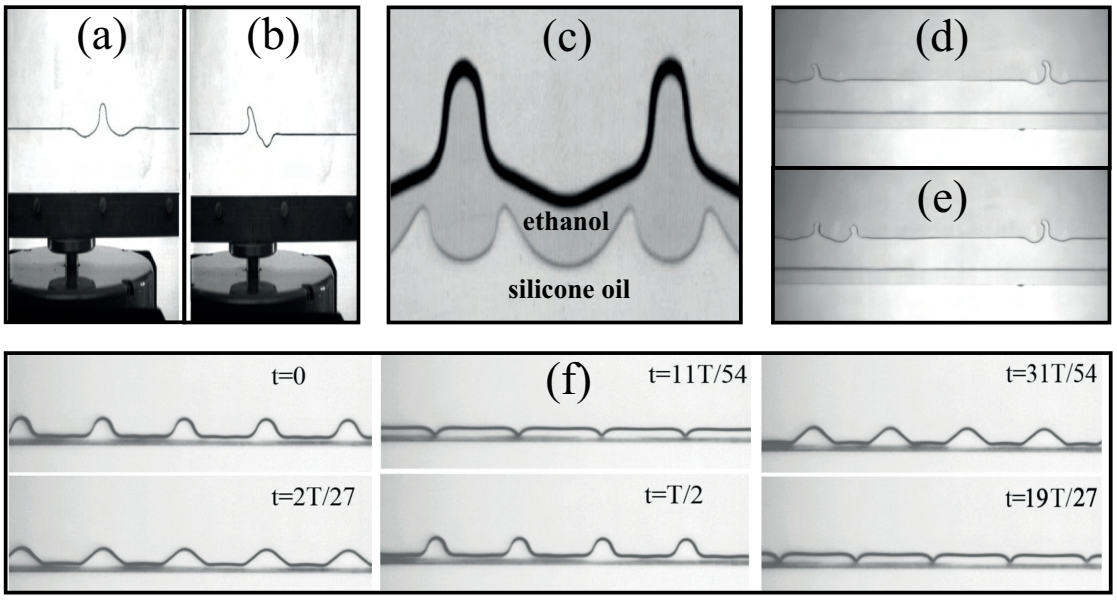

Figure III.4 – (a) Even and (b) odd standing solitary waves. Driving frequency, 11 Hz; vibration amplitude, 4.1 mm; the wave amplitudes are of the order of 1.2 cm (Rajchenbach et al., 2011). (c) The wave profile of two coupled Faraday waves observed in a two layers system of pure ethanol (depth $d_1 = 4$ mm) and silicone oil (depth $d_2 = 8$ mm) in the case of a forcing frequency of 18 Hz and acceleration 16 m/s^2 (Li et al., 2018b). (c,d) High localization of oscillons. Experiments were performed in 15% ethanol-water solution at a frequency of 18 Hz, an acceleration amplitude of 20.503 m/s^2, and a fluid depth of 2 cm. The right oscillon preserves the same structure in the (d) and (e). The left oscillon is single-peaked in the (d) but becomes double-peaked in the (e) by additional disturbance of the free surface (Li et al., 2014). (a)-(e) are experimental time snapshots. (f) Snapshots of the Faraday wave profiles in extreme shallow depth (2 mm) and observed for absolute ethanol at a forcing frequency of 18 Hz and forcing acceleration 19.80 m/s^2 (Li et al., 2015). In the various sub-panels, T denotes the wave period.

These findings represent a new contribution to the understanding of the wave behaviour in Hele-Shaw configurations. In this regard, it becomes therefore essential to have a reliable stability theory that can explain and predict the instability onset for the emergence of initial wave patterns.

Notwithstanding two-dimensional direct numerical simulations (Périnet et al., 2016; Ubal et al., 2003) have qualitatively reproduced standing wave patterns reminiscent of those observed experimentally (Li et al., 2014), ignoring the effect of internal wall attenuation leads to an oversimplified model that is not capable of quantitatively predicting the instability regions (Benjamin and Ursell, 1954; Kumar and Tuckerman, 1994a) and is not suitable for modelling Hele-Shaw flows. On the other hand, when attempting to perform three-dimensional simulations of fluid motions within a Hele-Shaw cell, one of the primary challenges that arises is the high computational cost associated with this task. Due to the small dimension in the narrow direction, the grid cell size must be set even smaller in order to accurately capture the

shear dissipation that occurs within the boundary layer. As a result, the computational cost of performing such simulations rapidly increases.

To overcome these challenges and arrive at a more accurate yet efficient approach for resolving the fluid dynamics within this system, researchers have largely invoked the use of Darcy's law to treat the confined fluid between two vertical walls as though it were flowing through a porous medium. When gap-averaging the linearized Navier-Stokes equation, this approximation, which assumes a steady parabolic flow in the short dimension, translates into a real-valued damping coefficient $\sigma \in \mathrm{R}$ that scales as $12\nu/b^2$, with ν the fluid kinematic viscosity and b the cell's gap-size, and which represents the boundary layer dissipation at the lateral walls. However, Darcy's model is known to be inaccurate when unsteady and convective inertias, e.g. through the advection of momentum, are not negligible, such as in waves (Kalogirou et al., 2016). It is not mathematically straightforward to consistently reintroduce convective terms in the gap-averaged Hele-Shaw equations (Plouraboué and Hinch, 2002; Ruyer-Quil, 2001).

Li et al. (2019) applied a Kelvin-Helmholtz-Darcy theory proposed by Gondret and Rabaud (1997) to reintroduce advection and obtain the nonlinear gap-averaged Navier-Stokes equations, which have been then implemented in the open-source code developed by (Popinet, 2003, 2009) to simulate Faraday waves in a Hele-Shaw cell. Although this gap-averaged model has been compared to several experiments showing fairly good agreements, the surface tension term is still two-dimensional, as the out-of-plane interface shape is not directly taken into account. This simplified treatment overlooks the contact line dynamics and may sometimes lead to miscalculations. Advances in this direction were made by Li et al. (2018a), who found that the out-of-plane capillary forces or curvature should be retained in order to improve the description of the wave dynamics, as experimental evidence suggests. By employing a more sophisticated model, coming from molecular kinetics theory (Blake, 1993, 2006; Hamraoui et al., 2000), to include the capillary contact line motion arising from the small scale of the gap-size between the two walls of a Hele-Shaw cell, they derived a novel dispersion relation, which indeed better predicts the observed instability onset.

Unfortunately, they couldn't exactly predict the exact instability thresholds as some discrepancies were still found. This mismatch was tentatively attributed to factors that are not accounted for in the gap-averaged model, such as the extra dissipation on the lateral walls in the elongated direction. Of course, a lab-scale experiment using a rectangular cell cannot entirely replace an infinite-length model, but if the container is sufficiently long, then this extra dissipation should be negligible. Other candidates were identified in the phenomenological contact line model or free surface contaminations.

If these factors can certainly be sources of discrepancies, our guess is that something more profound could be at the origin of the discordance between theory and experiments in the first place.

Despite the use of the Darcy approximation is well-assessed in the literature, the choice of a steady Poiseuille flow to build up the gap-averaged model appears in fundamental contrast with the unsteady nature of oscillatory Hele-Shaw flows, such as Faraday waves. At low enough oscillation frequency ω or for sufficiently viscous fluids, the thickness of the oscillating Stokes

boundary layer, $\delta' = \sqrt{2\nu/\omega}$, becomes comparable to the cell gap, b, i.e. $2\delta'/b \approx 1$: the Stokes layers over the lateral solid faces of the cell merge and eventually invade the entire fluid bulk. In such scenarios, the Poiseuille profile gives an adequate flow description, but this requisite is rarely met in the above-cited experimental campaigns. It appears, thus, very natural to ask oneself whether a more appropriate description of the oscillating boundary layer impacts the prediction of stability boundaries.

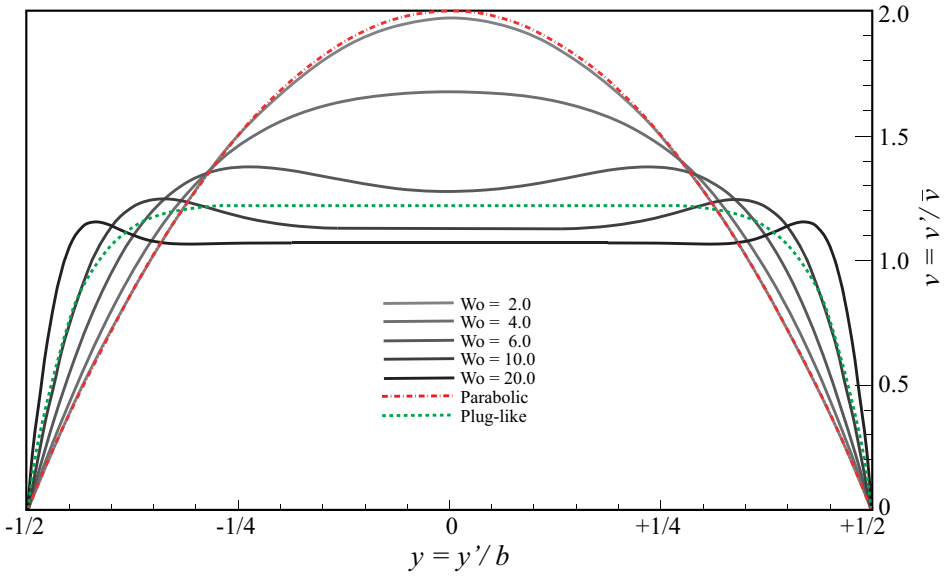

Figure III.5 – Womersley velocity profiles (modified figure from San and Staples (2012)) in a cell of width b and for different Womersley number $Wo = b\sqrt{2}/\delta'$. $\delta' = \sqrt{2\nu/\omega}$ denotes the Stokes boundary layer thickness and is a function of the fluid kinematic viscosity ν and the characteristic oscillation frequency of the flow ω. For $Wo \leq 2$, viscous forces dominate the flow, and the pulse is considered quasi-static with a parabolic profile. For $Wo \geq 2$ the inertial forces are dominant in the central core, whereas viscous forces dominate near the boundary layer. Thus, the velocity profile gets flattened, and the phase between the pressure and velocity gets shifted towards the core, with a complete phase opposition in the limit of a plug flow.

The study reported in **Chapter 8** is precisely devoted to answering this question by proposing a revised gap-averaged Floquet analysis, based on the classical Womersley-like solution for the pulsating flow in a channel (Womersley, 1955) (see figure III.5).
Following the approach taken by Viola et al. (2017), we examine the impact of inertial effects on the instability threshold of Faraday waves in Hele-Shaw cells, with a focus on the **unsteady term** of the Navier-Stokes equations. This scenario corresponds to a pulsatile flow where the fluid's motion reduces to a two-dimensional oscillating Poiseuille flow and it seems better suited than the steady Poiseuille profile to investigate the stability properties of the system. When gap-averaging the linearized Navier-Stokes equation, this results in a modified damping coefficient, a function of the ratio between the Stokes boundary layer thickness and the cell's gap, and whose complex value will depend on the frequency of the wave response specific to each unstable parametric region.

First, we consider the case of horizontally infinite rectangular Hele-Shaw cells by also accounting for the same dynamic contact angle model employed by Li et al. (2019), so as to quantify the predictive improvement brought by the present theory. A *vis*-à-vis comparison with experiments by Li et al. (2019) points out how the standard Darcy model often underestimates the Faraday threshold, whereas the present theory can explain and close the gap with these experiments.
The analysis is then extended to the case of thin annuli. This less common configuration has already been used to investigate oscillatory phase modulation of parametrically forced surface waves (Douady et al., 1989) and drift instability of cellular patterns (Fauve et al., 1991). For our interest, an annular cell is convenient as it naturally filters out the extra dissipation that could take place on the lateral boundary layer in the elongated direction, hence allowing us to reduce the sources of extra uncontrolled dissipation and perform a cleaner comparison with experiments. Our homemade experiments for this configuration highlight how Darcy's theory overlooks a frequency detuning that is essential to correctly predict the locations of the Faraday's tongues in the frequency spectrum. These findings are well rationalized and captured by the present model.